Quasiclassical Trajectory Study of the F + CH_4 Reaction Dynamics on a Dual-Level Interpolated Potential Energy Surface

J. F. Castillo,* F. J. Aoiz, and L. Bañares

Departamento de Química Física, Facultad de Química, Universidad Complutense, 28040 Madrid, Spain

E. Martinez-Nuñez, A. Fernández-Ramos, and S. Vazquez

Departamento de Química Física, Facultad de Química, Universidad de Santiago de Compostela, Santiago de Compostela, Spain

Received: April 22, 2005; In Final Form: July 26, 2005

An ab initio interpolated potential energy surface (PES) for the F + CH_4 reactive system has been constructed using the interpolation method of Collins and co-workers. The ab initio calculations have been performed using second-order Möller−Plesset (MP2) perturbation theory to build the initial PES. Scaling all correlation (SAC) methodology has been employed to improve the ab initio calculations and to construct a dual-level PES. Using this PES, a detailed quasiclassical trajectory study of integral and differential cross sections, product rovibrational populations and internal energy distributions has been carried out for the F + CH_4 and F + CD_4 reactions and the theoretical results have been compared with the available experimental data.

I. Introduction

The reaction

$$F(^2P) + CH_4(X\ ^1A_1) \rightarrow HF(X\ ^1\Sigma^+) + CH_3(X\ ^2A'') \qquad \Delta_r H_o^{\ominus} = -32.0 \text{ kcal mol}^{-1} \quad (1)$$

has been studied in detail experimentally and less exhaustively theoretically over recent years. The first experimental study of the F + CH_4 product energy distribution under low-pressure conditions was carried out by Nazar and Polanyi[1] by measuring infrared chemiluminescence of the HF products. These experiments revealed a highly inverted vibrational distribution of the HF products and rotational populations for each vibrational state well reproduced by Boltzmann distributions at 300 K. Similar vibrational and rotational distributions were measured by Wickramaaratchi et al.[2] using FTIR detection of the HF products. However, these experimental studies were not performed under single collision conditions and the possibility of partial rotational relaxation of the nascent HF products and secondary reactions could not be ruled out. Recently, Nesbitt and co-workers[3,4] have investigated the quantum state resolved dynamics of the F + $CH_4 \rightarrow HF(v, j) + CH_3$ reaction under crossed supersonic jet conditions, which neatly eliminate contributions from collisional relaxation effects and secondary reactions, using high-resolution IR laser absorption techniques. The observed HF vibrational energy distribution at a collision energy of 1.8 kcal mol^{-1} is in very good agreement with those obtained previously.[1,2] However, the rotational distributions were found to be consistently broader in all vibrational states than the earlier rotational distributions measured by Wickramaartachi et al.,[2] and especially for $v' = 1$, where the previous distribution peaks at $j' = 2$ whereas that measured by Nesbitt and co-workers peaks at $j' \approx 8$. The differences were attributed to partial thermal equilibration, in the work of ref 2, for low rotational levels. Experimental vibrational and rotational energy distributions of the CH_3 coproduct of the title reaction at translational energies around 2.6 kcal mol^{-1} were first measured by Sugawara et al.[5] in a bulk experiment using time-resolved diode laser absorption spectroscopic detection of CH_3. They concluded that nascent CH_3 is produced rotationally cold and only 3% and 2% of the total available energy is channelled into the v_2 vibrational mode and rotation of the CH_3 product, respectively. From all these previous experimental studies, the energy partitioning into vibration and rotation of the HF and CH_3 products can be summarized as[7] $f_v(HF) = 0.61$, $f_r(HF) = 0.03$, $f_v(CH_3(v_2)) = 0.03$, and $f_r(CH_3) = 0.02$.

Very recently, a series of sophisticated experiments that have provided outstanding information on the reaction dynamics of the F + CH_4 reaction have been carried out by Liu and co-workers.[6−12] Using a rotating-source crossed molecular beam apparatus in combination with time-sliced velocity map imaging, correlated information of coincident product pairs could be obtained, extracting the very fine details of the dynamics of the title reaction and of the F + CD_4 and F + CHD_3 isotopic variants. In particular, state-specific excitation functions for the formation of $CD_3(v_2 = 0, 1, 2, 3)$ products[7] and state-resolved, pair-correlated differential cross sections (CDCS)[6,8,11] were measured for the F + CD_4 reaction at several collision energies in the range 0.5−7.5 kcal mol^{-1}. It was found that ≈6−8% of the total available energy appears as CD_3 internal energy. About 4% of the energy goes into vibrational energy of CD_3 (only the v_2 umbrella mode of CD_3 molecule is active in the reaction) and, although the rotational excitation of CD_3 is small, a strong preference for $K = 0$ was found, indicating a dominance of tumbling rotational motion of the CD_3 product. These studies revealed that the correlated integral cross sections (CICS) and CDCS depend on the final CD_3 quantum state selected. Besides, the vibrationally state-specific excitation function for the F + $CH_4 \rightarrow HF(v') + CH_3(v = 0)$ reaction was measured in the collision energy range 0.5−7.5 kcal mol^{-1}.[9] The reaction

* Author for correspondence. E-mail: jfc@legendre.quim.ucm.es.

10.1021/jp052098f CCC: $30.25
Published on Web 09/07/2005

exhibits a threshold of ≈0.56 kcal mol^{-1} and after threshold the excitation function shows a peak at ≈2.5 kcal mol^{-1} and then declines. Only the HF($v' = 2, 3$) quantum states are populated and the v' state resolved excitation functions also show a maximum and a decline, especially for $v' = 3$. Interestingly, the results obtained for the vibrational branching ratios were not inconsistent with those reported previously.[1−3] A very intriguing and remarkable finding for the F + CH_4 reaction was that the $CH_3(v = 1)$ product state is noticeably populated near threshold and shows a rapidly declining population function.[10] In addition, the appearance of $CH_3(v = 0)$ is correlated with a broad rotational distribution of HF($v' = 2, j'$). These unexpected features are reminiscent of those observed for the F + HD → HF + D reaction and have been taken as evidence for the existence of a reactive resonance in this six-atom reaction.[10] Moreover, the two channel F + CHD_3 reaction was investigated at collision energies in the range 0.4−7.5 kcal mol^{-1}. The excitation function corresponding to the HF(v') + $CD_3(v = 0)$ channel exhibits a steplike structure near the threshold, which resembles that found in the F + HD → HF(v') + D reaction and suggests the existence of a reactive resonance.[12]

From the theoretical side the number of studies of the F + CH_4 reaction is relatively scarce.[13−16,18] The first theoretical ab initio study of the stationary points and reaction path of the FCH_4 potential energy surface (PES) was carried out by Corchado and Espinosa-García[13,14] using second-order Möller−Plesset pertubation theory (MP2) and quadratic configuration interaction with single and double excitations (QCISD). The calculations at the MP2/6-31G(d,p) and QCISD/6-31G(d,p) levels of theory predicted a nonlinear F−H−CH_3 transition state (F−H−C angle of 161°) located at the entrance valley. Higher level calculations using QCISD(T)/6-311++G(3df,2p) yielded an enthalpy of reaction in very good agreement with the experimental value of 32.0 kcal mol^{-1} [19] and the calculated classical barrier height was 0.96 kcal mol^{-1} with a zero-point-energy (ZPE) corrected barrier height of −1.93 kcal mol^{-1}.[13,14] Following that study, Corchado and Espinosa-García[14] developed two semiempirical PESs: one using the PM3 semiempirical approach with specific reaction parameters (SRP), named PM3-SRP, and the other by modifying several parameters of the J1 PES for the well studied H + CH_4 reaction,[20] named MJ1 PES. Both PESs exhibit an early linear transition state with classical barriers of 2.39 and 1.00 kcal mol^{-1} for the PM3-SRP and MJ1 PESs, respectively. Both semiempirical surfaces showed similar room-temperature kinetic isotope effect (KIE) (≈2.3), calculated using variational transition state theory, in qualitative agreement with experiment (1.4).[2] However, none of these PESs has been employed in any dynamical calculation. Okuno and co-workers[16] performed ab initio calculations using MP2/cc-pVTZ theory. Their calculations predicted a linear transition state located 4.47 kcal mol^{-1} above reactants. Very recently, Espinosa-Garcia et al.[17] built an analytical symmetric PES for the F + CH_4 reaction calibrated with respect to the updated experimental and theoretical stationary point properties and thermal rate constants. In fact, two versions of the PES were produced: the PES−SO version that takes as zero reference level the spin−orbit ground state of F atom ($^2P_{3/2}$) and the PES-NOSO version that takes as zero reference level the average energy of the two spin−orbit states of the F atom. They used the improved canonical version of the variational transition state theory with microcanonical optimized multidimensional tunneling to compute the rate constants and concluded that the PES-NOSO yielded better agreement with the experimental rate constants. The PES-NOSO exhibits a classical barrier height of 0.25 kcal mol^{-1} with a zero-point-energy (ZPE) corrected barrier height of −0.45 kcal mol^{-1}.

The first quasiclassical trajectory (QCT) dynamical calculation for the F + CH_4 reaction was carried by Kornweitz et al.[15] using a modified version of the J1 PES.[20] The calculated HF vibrational energy distribution agrees relatively well with the experimental determinations mentioned above.[1,2,3] Very recently, Troya et al.[18] performed detailed ab initio calculations and developed an analytical reduced dimensionality PES for the FCH_4 system treating the CH_3 group as a pseudoatom. Their highest level of ab initio theory QCISD(T)//QCISD/6-311+G-(2df,2pd) yielded a classical barrier height of 0.46 kcal mol^{-1} (and a ZPE corrected barrier of −0.65 kcal mol^{-1}). In all cases, the saddle point was found to be linear. The PES was constructed by fitting the ab initio points calculated at the PUMP4/6-311+(2df,2pd) level of theory to a triatomic analytical representation. The corresponding QCT calculations predicted HF vibrational energy distribution in good agreement with experiments and HF rotational populations in accordance with the determinations of Harper et al.[3]

To our knowledge, a fully ab initio global PES is not available for the title reaction. In this work, we have carried out an ab initio study of the FCH_4 system. A ab initio PES has been developed using the iterative interpolation method devised by Collins and co-workers[21−24] and recently implemented in the GROW package. The constructed PES is based on MP2/aug-cc-pVDZ ab initio calculations. In addition, the scaling all correlation (SAC) methodology has been employed to improve the ab initio points and to construct dual-level PESs. QCT dynamical calculations have been carried out on these PESs and on the PES-NOSO constructed by Espinosa-García and co-workers.[17] The present theoretical results have been compared with the experimental data available.

II. Ab Initio Calculations and Potential Energy Surfaces

The ab initio calculations have been carried out using the GAUSSIAN 98 suite of programs.[25] We have performed an ab initio study of the stationary points relevant to the reaction using UHF, MP2, QCISD, and QCISD(T) employing different correlation consistent basis sets.[26] The calculations of the transition state geometry and reaction paths have been performed in the C_{3v} symmetry. For the QCISD(T) calculations, the geometry employed was optimized and the frequencies calculated at the QCISD level of theory using different basis sets. Table 1 shows the relative energies of the stationary points, including the F−H−CH_3 transition state, the HF + CH_3 asymptote and the reactant and product van der Waals minima, with respect to the F + CH_4 asymptote and including zero-point energy (ZPE) corrections.

From the values listed in Table 1, several observations can be made regarding the QCISD and QCISD(T) calculations. (1) The inclusion of triple excitations, QCISD(T), for a given basis set, brings down the barrier height by about 1 kcal mol^{-1} with respect to the values predicted by the QCISD method. (2) The augmented basis sets yield lower barriers than those calculated using nonaugmented basis sets. In fact, the augmented basis set calculations predict negative ZPE corrected barriers. The experimental activation energy and threshold energy for the F + CH_4 → HF + $CH_3(000)$ reaction are fairly small, ≈0.5 kcal mol^{-1}. The calculation QCISD(T)//QCISD/cc-pVTZ, yields a ZPE corrected barrier in good agreement with the experimental estimates. The MP2/aug-cc-pVDZ calculation gives a ZPE corrected barrier somewhat higher than the experiments, but still in good agreement (within 1 kcal mol^{-1} difference). The

TABLE 1: Energies of the Stationary Points of the F + CH_4 ($^2A_1$) PES Including the Zero-Point Energy Correction[a]

method	F−H−CH_3 (TS)	HF + CH_3
QCISD/cc-pVDZ	2.43 (5.14)	−22.12 (−18.45)
QCISD(T)//QCISD/cc-pVDZ	1.70 (4.40)	−22.05 (−18.37)
QCISD/aug-cc-pVDZ	−0.28 (0.97)	−29.94 (−26.48)
QCISD(T)//QCISD/aug-cc-pVDZ	−1.08 (0.17)	−30.18 (−26.72)
QCISD/cc-pVTZ	1.13 (2.65)	−28.43 (−24.96)
QCISD(T)//QCISD/cc-pVTZ	0.13 (1.65)	−29.16 (−25.70)
QCISD/aug-cc-pVTZ//QCISD/cc-pVTZ	−0.77 (0.76)	−30.82 (−27.35)
QCISD(T)/aug-cc-pVTZ//QCISD/cc-pVTZ	−2.15 (−0.63)	−31.64 (−28.18)
MP2/aug-cc-pVDZ	1.44 (3.44)	−35.27 (−31.78)
MP2/cc-pVTZ	2.47 (4.47)	−34.00 (−30.40)
MP-SAC2 ($F = 0.87$)	0.49 (2.14)	−38.40 (−34.89)
MP-SAC2 ($F = 0.82$)	0.11 (1.61)	−39.77 (−36.33)
MP-SAC2 ($F = 0.78$)	−0.10 (1.18)	−40.91 (−37.63)
MP-SAC2 ($F = 0.76$)	−0.25 (0.96)	−41.71 (−38.31)
experiment	0.8 ± 0.3[b] (0.54)[c] (0.50)[d]	−32.10,[e] (−28.5)[f]
	vdW Reactant Minimum	
QCISD/aug-cc-pVDZ		−0.10 (−0.33)
MP2/aug-cc-pVDZ		−0.01 (−0.23)
	vdW Product Minimum	
QCISD/aug-cc-pVDZ		−30.69 (−28.76)
MP2/aug-cc-pVDZ		−36.16 (−34.19)

[a] All energies are in kcal mol^{-1} relative to F + CH_4 reactants. The values in parentheses correspond to classical energies. [b] Energy of activation from an Arrhenius fit of rate constants ref 18. [c] Energy of activation from ref 46. [d] Energy threshold for the F + $CH_4 \rightarrow$ HF + CH_3(000) reaction, ref 9. [e] Reference 47. [e] Calculated as $\Delta E + \Delta ZPE$.

TABLE 2: Geometries of the Saddle Point and Product Valley Minimum of the F + CH_4 ($^2A_1$) PES

saddle point	$R_{H'-F}$/Å	$R_{H'-C}$/Å	R_{H-C}/Å	$\angle_{F-H'-C}$/deg	$\angle_{H-C-H}$/deg
UHF/aug-cc-pVDZ	1.250	1.220	1.085	180.00	104.94
QCISD/cc-pVDZ	1.376	1.160	1.100	180.00	106.81
QCISD/aug-cc-pVDZ	1.586	1.127	1.100	180.00	107.67
QCISD/cc-pVTZ	1.483	1.124	1.086	180.00	107.40
MP2/aug-cc-pVDZ	1.466	1.137	1.096	180.00	107.12
MP2/cc-pVTZ	1.433	1.126	1.083	180.00	107.23
MP-SAC2 ($F = 0.78$)	1.564	1.124	1.099	180.00	107.76
		vdW Product Minimum			
QCISD/aug-cc-pVDZ	0.928	2.286	1.093	180.00	93.22
MP2/aug-cc-pVDZ	0.931	2.256	1.089	180.00	93.30
MP−SAC2	0.942	2.387	1.092	180.00	93.48

TABLE 3: Frequencies in cm^{-1} of the Saddle Point of the F + CH_4 ($^2A_1$) PES

	UHF/aug-cc-pVDZ	QCISD/aug-cc-pVDZ	QCISD/cc-pVTZ	MP2/aug-cc-pVDZ	MP-SAC2
ω_1, ω_1 (E)	3341.6	3182.6	3196.6	3241.3	3219.6
ω_3 (A_1)	3203.7	3070.8	3086.9	3108.7	3083.7
ω_4 (A_1)	1529.5	2443.5	2124.5	1914.6	2486.6
ω_5, ω_6 (E)	1347.7	1477.6	1501.4	1476.1	1458.4
ω_7, ω_8 (E)	1238.8	1268.4	1280.1	1245.7	1230.7
ω_9 (A_1)	605.6	1266.9	1277.5	1218.3	1230.6
ω_{10}, ω_{11} (E)	332.0	27.8	78.5	94.2	85.2
ω_{12} (A_1)	2949.4i	250.9i	371.9i	606.4i	327.5i

geometries of the saddle point calculated a several levels of ab initio theory are presented in Table 2. All calculations yield a linear F−H′−C transition state (TS) geometry in accordance with previous ab initio studies.[16,18] The $R_{H'-F}$ and R_{H-C} distances and the $\angle_{H-C-H}$ angle indicate that the TS geometry is closer to reagents than to products; i.e., the PES is characterized by an early barrier. Interestingly, with the QCISD/aug-cc-pVDZ method the $R_{H'-F}$ distance is about 0.1 Å larger than that determined with the cc-pVTZ basis. This fact is consistent with the lower barrier for the reaction predicted by the QCISD/aug-cc-pVDZ in comparison with the QCISD/cc-pVTZ calculation. Harmonic frequencies calculated for the TS are presented in Table 3. Note the rather small value of the imaginary frequency obtained with QCISD and MP2 methods, which is consistent with the relatively large $R_{H'-F}$ distance.

The calculated exothermicity at 0 K using QCISD(T) and basis sets larger than cc-pVDZ (Table 1) are in relative agreement with the experimental value (within a difference no larger than 3 kcal mol^{-1} or 9%). The MP2 method overestimates the experimental value by nearly 3 kcal mol^{-1}. As in previous studies,[18] we have been able to calculate the geometry and energy of a C_{3v} van der Waals minimum in the product valley (see Tables 1 and 2). The predicted depth of the well is about 2.4 kcal mol^{-1} relative to products using QCISD and MP2 methods with aug-cc-pVDZ basis set, respectively. Additionally, we have located a shallow C_{3v} van der Waals minimum in the reactant valley. The geometry and energy of van der Waals minima have been calculated including the basis set superposition error using the "counterpoise" method implemented in Gaussian.[25]

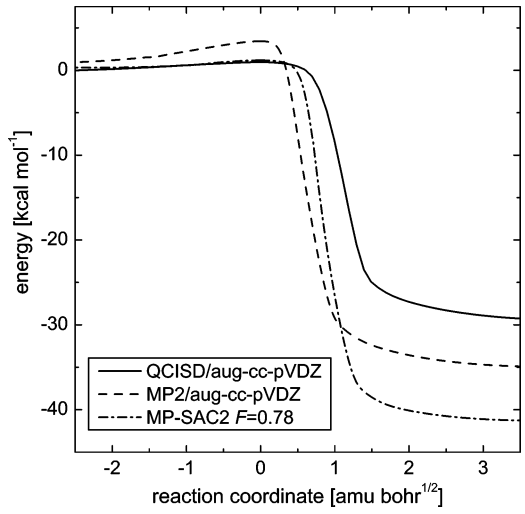

Figure 1. Minimum energy path (MEP) for the F + CH_4 → HF + CH_3 reaction. Solid line: QCISD/aug-cc-pVDZ level of theory. Dashed line: MP2/aug-cc-pVDZ. Dotted line: MP-SAC2 $F = 0.78$.

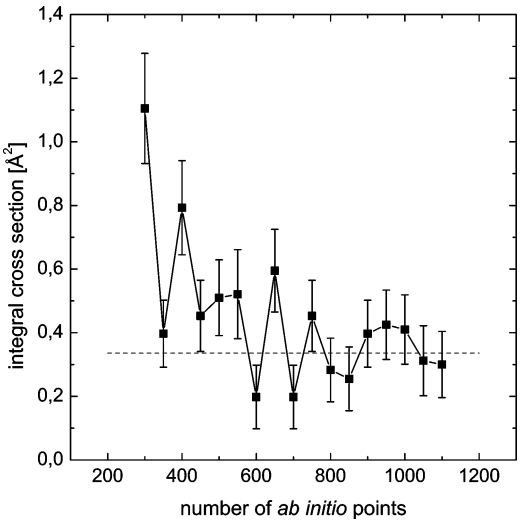

Figure 2. Convergence of the total reaction cross section (in Å^2) as a function of the number of data points calculated employing the GROW script and VENUS96 programs using the MP2/aug-cc-pVDZ level of theory for the F + CH_4 → HF + CH_3 reaction at a collision energy of 4 kcal mol^{-1} (see text for more details). The horizontal dashed line corresponds to the average value of the cross section for a number of data points larger than 800.

Tables 4−6 show the frequencies and geometries of the CH_4, CH_3, and HF molecules calculated at various levels of theory. As can be seen, the QCISD/cc-pVTZ method provides the best agreement with the experimental geometries and frequencies for these molecules.

From the F−CH_4 transition state, the intrinsic reaction coordinate (IRC) or minimum energy path (MEP) has been calculated at the QCISD/aug-cc-pVDZ and MP2/aug-cc-pVDZ levels of theory using the Berny algorithm implemented in GAUSSIAN 98.[25] The MEPs are displayed in Figure 1. The energy profile in the reactant region is very flat, as observed in other earlier works.[13,16,18,17] Although it is not shown in Figure 1, it is interesting to note that the MEP that connects the TS with reactants leads to the shallow C_{3v} van der Waals minimum in the reactant valley mentioned above. As can be seen, the MP2/aug-cc-pVDZ MEP shows a larger barrier and exothermicity in comparison with the MEP calculated at the QCISD/aug-cc-pVDZ level of theory. In addition, after the saddle point, the former goes down toward the negative energy corresponding to the reaction exothermicity much faster than the latter. It is expected that these two facts will have important repercussions in the dynamics of the title reaction.

In this work, the aim has been to construct a full dimensional ab initio PES for the study of the dynamics of the title reaction. For the construction of the PES, the interpolation method developed by Collins et al.[21,22,23,24] has been employed. The method requires the calculation of energies, gradients, and Hessians of a relatively large set of ab initio points. According to the ab initio calculations presented above, the QCISD(T)//QCISD/cc-pVTZ method renders relative energies and geometries in good agreement with the experimental information. However, the QCISD(T)//QCISD/cc-pVTZ method is computationally very expensive for the construction of the PES for the FCH_4 system. A single point calculation of energy, gradients, and Hessians using QCISD/cc-pVTZ level takes up to 31 h of CPU time on a DEC 2650 Alpha server. Although the MP2/aug-cc-pVDZ method yields an energy barrier and exothermicity that are too high in comparison with the experimental data, it has the advantage that the computational effort is affordable and that gradients and Hessians can be calculated analytically. Therefore, the MP2/aug-cc-pVDZ method has been chosen to construct the PES. The set of points that define the reaction path shown in Figure 1 have been used to calculate the initial surface. A total of 100 points for the reaction path have been calculated and used as initial guess for developing the PES. The self-consistent field (SCF) wave function has been required to be converged tightly to 10^{-10} hartree and to be stable for all points. The PES has been grown using the iterative methods implemented in the GROW script, using the MP2/aug-cc-pVDZ ab initio level of theory. The methods for choosing a new data point at each iteration have been discussed in detail elsewhere. The "variance sampling"[27] and "h weight" methods[28,29] have been used alternatively for each additional data point. The classical trajectory calculations, which are performed to select new data points, have been run under the following conditions with the VENUS96 program[30] (note that the QCT code employed is not the code incorporated in the original GROW script). A ground state zero-point energy has been given to CH_4 with coordinates and momenta corresponding to a fixed microcanonical normal mode sampling. A relative translational energy of 4.0 kcal mol^{-1} and a maximum impact parameter of 2.5 Å were chosen for the initial conditions of the trajectories. Both the initial and final relative separations of the F-atom to the CH_4 molecule and of the HF and CH_3 products, respectively, were set to 7 Å. A total of 1100 data points, which include energy and the first and second derivatives, have been calculated for the present PES. The convergence of the total integral cross section has been monitored while the surface was being developed by running batches of 1000 trajectories. Figure 2 shows the total cross section for the reaction as a function of the size of the data set that defines the interpolated PES. The cross section only changes by less than 5% when the number of ab initio points is increased from 1000 to 1100.

To obtain a PES with a lower energy barrier, we have employed the scaling all correlation (SAC) method of Truhlar et al.[31,32] Very recently, this type of scaling has been used in direct dynamics QCT calculations of the O(^{1}D) + CH_4 reaction.[33] The energy $E_{MP-SAC2}$ of the scaled PES is given by

$$E_{MP-SAC2} = E_{HF} + \frac{E_{MP2} - E_{HF}}{F} \qquad (2)$$

where E_{HF} is the Hartree−Fock energy and F is a global constant. Gradients and Hessians are calculated by direct

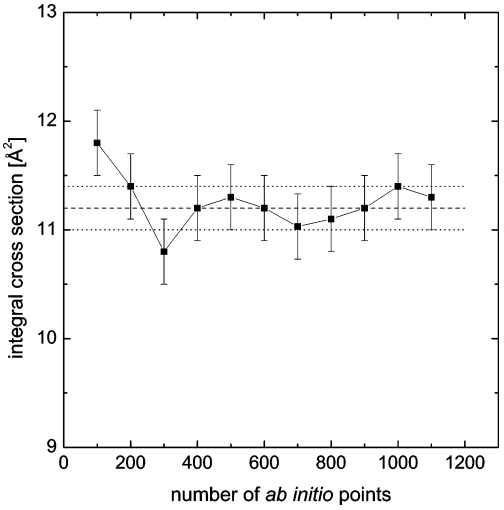

Figure 3. Convergence of the total reaction cross section (in Å^2) as a function of the number of data points calculated employing the GROW script and VENUS96 programs using the MP-SAC2 PES for the F + $CH_4 \rightarrow$ HF + CH_3 reaction at a collision energy of 8 kcal mol^{-1} (see text for more details). The horizontal dashed line corresponds to the average value of the cross section for a number of data points larger than 800. Dotted lines represent the average value ±2%.

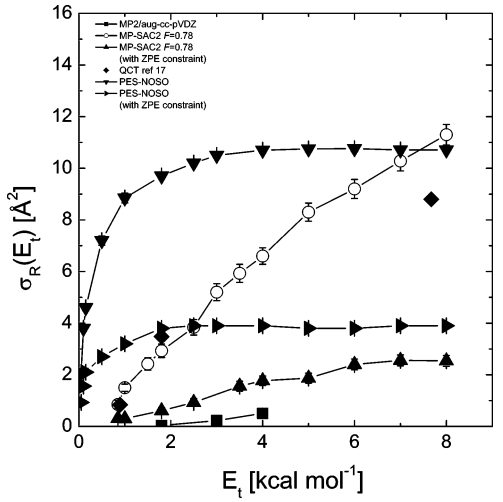

Figure 4. Excitation function for the F + $CH_4 \rightarrow$ HF + CH_3 reaction. Solid line with circles: QCT results using MP-SAC2 $F = 0.78$ PES. Solid line with squares: QCT results using the interpolated MP2/aug-cc-pVDZ PES. Solid line with triangles down: QCT results using the PES-NOSO surface.[17] Solid line with triangle: QCT results using MP-SAC2 $F = 0.78$ PES and considering only those reactive trajectories yielding CH_3 products with internal energy no larger than the ZPE. Black diamonds: QCT results from ref 18. Solid lines with triangles right: QCT results using PES-NOSO surface.

differentiation of eq 2. To construct a MP-SAC2 interpolated PES, E_{MP2} and E_{HF} have to be interpolated at the same geometries. Thus, HF/aug-cc-pVDZ energies, gradients, and Hessians have been calculated at the same ab initio points that define the interpolated MP2/aug-cc-pVDZ PES. The value of the constant $F = 0.78$ has been chosen to obtain a threshold energy of about 0.5 kcal mol^{-1} from the QCT calculations (see Figure 4 and section 4). For $F = 0.78$, the classical barrier energy is 1.18 kcal mol^{-1} and the ZPE corrected barrier is −0.1 kcal mol^{-1} (see Table 1). Unfortunately, the MP-SAC2 PES with $F = 0.78$ yields a reaction exothermiticy of 40.91 kcal mol^{-1} to be compared with the experimental value of 32 kcal mol^{-1}. Tables 1−6 show the stationary points properties obtained for the MP-SAC2 PES with $F = 0.78$. Table 1 also lists the saddle point energies and exothermicities obtained for other values of F within the range 0.76−0.87. The different values of F yield ZPE corrected barrier heights and exothermicities in the ranges −0.25 to +0.49 kcal mol^{-1} and −41.71 to −38.40 kcal mol^{-1}, respectively. Figure 3 shows the variation of the total integral cross section with the number of data points included in the MP-SAC2 PES with $F = 0.78$ for a collision energy of 8 kcal mol^{-1}. Batches of 4000 trajectories have been run for each set of data points. As can be seen, the ICS converges with the number of data points within a variation of 2%.

III. Quasiclassical Trajectory Method

The methodology used in the present QCT calculations is similar to that described in recent studies of the H + H_2O[34,35] and H + N_2O[36,37] reactions. Initial conditions for the rotationless CH_4 molecule in its vibrational ground state has been chosen using fixed normal mode energy sampling.[30] The impact parameter has been chosen randomly between 0 and 3.5 Å and the initial distance between the F atom and the C atom of the CH_4 molecule has been set to 8 Å. A integration time step of 0.04 fs has been used, which yields a conservation of the total energy better than 1 in 10^4. For the HF or DF product the rotational quantum number is obtained by equating the square modulus of the classical rotational angular momentum to $[j'(j'+1)]^{1/2}\hbar$. The (real) j' value so obtained is rounded to the nearest integer. The vibrational quantum number is found by Einstein−Brillouin−Keller (EBK) semiclassical quantization of the action integral.[30] For the CH_3 coproduct the instantaneous rotational energy has been calculated as $E_r = {}^1/_2\vec{\omega}\cdot\vec{j}$ and the vibrational energy is given by $E_v = E_{int} - E_r$, where E_{int} is the total internal energy of the product. A batch of 5×10^4 trajectories at the collision energy $E_t = 1.8$ kcal mol^{-1} of the experiments of Harper et al.[3] and batches of 4000 trajectories have been run at $E_t = 3.0$ and 4.0 kcal mol^{-1} on the interpolated MP2/aug-cc-pVDZ ab initio PES. A batch of 25 000 trajectories at $E_t = 1.8$ kcal mol^{-1} and batches of 2000 trajectories for $E_t = 0.5-8$ kcal mol^{-1} have been run using the MP-SAC2 PES with a scaling constant of $F = 0.78$. For the F + CD_4 reaction a batch of 13 000 trajectories has been run at $E_t = 5.4$ kcal mol^{-1} and batches of 2000 trajectories have been calculated in the range of collision energies of $E_t = 0.5-8$ kcal mol^{-1}. Using the PES-NOSO surface,[17] we have run batches of 20 000 trajectories per collision energy for the F + CH_4 and F + CD_4 reactions in the range $E_t = 0.05-8$ kcal mol^{-1}. Note that calculations using the PES-NOSO surface can be carried out about 10 times faster than using the MP2 or MP-SAC2 interpolated PES's.

The DCSs have been derived by employing the method of moments expansion in Legendre polynomials. The Smirnov−Kolmogorov test is used to decide when to truncate the series. Significance levels higher that 95% can be achieved using 5−6 moments, ensuring good convergence, such that the inclusion of more terms does not produce significant change.

IV. Results and Discussion

A. Excitation Functions. Figure 4 shows the QCT excitation function, i.e., the integral cross section as a function of the collision energy, $\sigma_R(E_t)$, for the series of PESs used in the present work. In particular, the cross sections have been calculated at 1.8, 3.0, and 4.0 kcal mol^{-1} collision energies on the interpolated MP2/aug-cc-pVDZ PES without any external scaling. As can be seen, the QCT calculation predicts a reaction threshold of ≈1.5 kcal mol^{-1}, which is 1.0 kcal mol^{-1} higher than the experimentally obtained by Shiu et al.[9] It should be remembered that in the experiments of Liu and co-workers, the

TABLE 4: Frequencies in cm^{-1} and Geometries in Å of the CH_4 ($^1A_1$)

	UHF/aug-cc-pVDZ	QCISD/aug-cc-pVDZ	QCISD/cc-pVTZ	MP2/aug-cc-pVDZ	MP-SAC2	experiment[a]
ω_1 (T_2)	3266.0	3153.0	3161.7	3208.5	3188.5	3019.5
ω_3 (A_1)	3152.7	3027.4	3044.8	3064.8	3033.5	2916.5
ω_4 (E)	1637.6	1543.9	1580.8	1550.6	1522.2	1533.3
ω_5 (T_2)	1423.6	1330.2	1356.6	1323.4	1290.3	1310.8
R_{H-C}	1.089	1.102	1.088	1.098	1.101	1.091
$\angle_{H-C-H}$	109.5	109.5	109.5	109.5	109.5	109.5

[a] Experimental data from ref 19.

TABLE 5: Frequencies in cm^{-1} and Geometries in Å of the CH_3 ($^2A''_2$)

	UHF/aug-cc-pVDZ	QCISD/aug-cc-pVDZ	QCISD/cc-pVTZ	MP2/aug-cc-pVDZ	MP-SAC2	experiment[a]
ω_1 (E′)	3421.0	3302.1	3318.0	3364.5	3349.6	3184.0
ω_3 (A'_1)	3233.7	3114.2	3137.6	3165.1	3136.7	3002.0
ω_4 (E′)	1496.6	1413.1	1434.6	1424.5	1380.1	1383.0
ω_5 (A''_2)	420.3	496.7	489.5	494.7	521.0	580.0
R_{H-C}	1.079	1.092	1.077	1.088	1.090	1.077
$\angle_{H-C-H}$	120.0	120.0	120.0	120.0	120.0	120.0

[a] Experimental data from ref 19.

TABLE 6: Frequencies in cm^{-1} and Geometries in Å of the HF ($^1\Sigma^+$)

	UHF/aug-cc-pVDZ	QCISD/aug-cc-pVDZ	QCISD/cc-pVTZ	MP2/aug-cc-pVDZ	MP-SAC2	experiment[a]
ω	4467.2	4103.6	4203.5	4083.2	3964.9	4138.5
R_{HF}	0.900	0.923	0.916	0.925	0.933	0.917

[a] Experimental data from ref 19.

pair-correlated excitation function of the F + CH_4 → HF(v' = 2, 3) + CH_3(v = 0) reaction was measured. The resulting total experimental excitation function summed on vibrational states of the HF product shows a rapid increase from threshold up to $E_t \approx 2.5$ kcal mol^{-1} and then a decline as collision energy increases. The QCT excitation function calculated on the MP2/aug-cc-pVDZ PES is much less steep than the experimentally observed and it does not show the prominent maximum at $E_t \approx 2.5$ kcal mol^{-1}. The discrepancies found between theory and experiment can be attributed to the apparently high energy barrier of the present interpolated PES calculated at the MP2/aug-cc-PVDZ level of theory.

As mentioned in section II, the barrier height of the interpolated PES has been reduced by using the SAC methodology. Several dual-level MP-SAC2 interpolated PESs were generated for different values of the F parameter in eq 2. A value of $F = 0.78$ was finally selected to obtain a threshold of ≈0.5 kcal mol^{-1} from the QCT calculations, although with this F value an exothermicity of 40.91 kcal mol^{-1} was obtained, at variance with the experimental value of 32.0 kcal mol^{-1}. Figure 4 depicts the excitation function calculated on the dual-level MP-SAC2 $F = 0.78$ PES (open circles). Given the smaller barrier to reaction of the MP-SAC2 $F = 0.78$ PES, the values of the integral cross sections (ICS) are significantly larger than those obtained on the interpolated MP2/aug-cc-pVDZ PES. As can be seen, the threshold is now close to 0.5 kcal mol^{-1}, but the reaction cross section always rises in the collision energy range from threshold up to 8 kcal mol^{-1}, showing no maximum, at variance with the experimental result. The calculated excitation function using the PES-NOSO surface shows a fast rise near the threshold and then levels off for collision energies above 2.5 kcal mol^{-1}, which differs as well from the experimental excitation function. The QCT ICS calculations for the F + CH_4 reaction by Troya et al.[18] (solid diamonds) have also been included for comparison.[38] There is good agreement between the ICSs obtained from both sets of QCT calculations at collision energies below 2 kcal mol^{-1}. However, at $E_t \approx 8$ kcal mol^{-1} the ICS calculated in ref 18 is significantly smaller than the present one. The present QCT excitation function considering only trajectories that lead to CH_3 products with internal energy below or equal its ZPE (solid triangles), which would correspond to the experimental excitation function producing CH_3(v = 0) molecules measured by Shiu et al.,[9] yields ICSs significantly smaller than those obtained when considering all CH_3 products and a similar shape, without showing any maximum at $E_t \approx$ 2.5 kcal mol^{-1}.

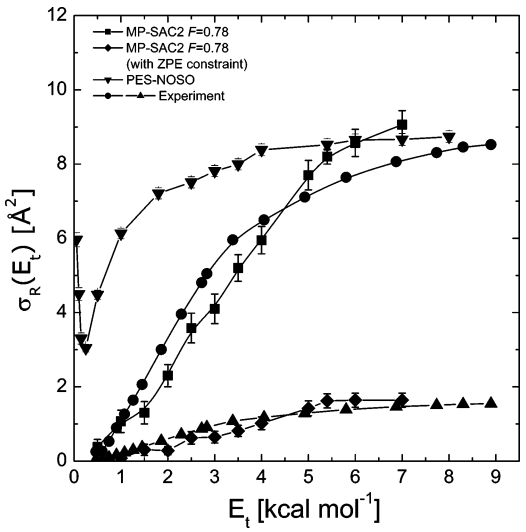

Figure 5. Excitation function for the F + CD_4 → DF + CD_3 reaction. Solid line with squares: QCT results using the MP-SAC2 $F = 0.78$ PES. Solid line with triangles down: QCT results using the PES-NOSO surface.[17] Solid line with diamonds: QCT results using the MP-SAC2 $F = 0.78$ PES and considering only those reactive trajectories yielding CD_3 products with internal energy no larger than the ZPE. The experimental data from ref 7 have been scaled to the QCT results obtained on the MP-SAC2 $F = 0.78$ PES without (solid line with circles) and with (solid line with triangles) ZPE constraints imposed on the CH_3 product.

The QCT $\sigma_r(E_t)$ values calculated on the dual-level MP-SAC2 $F = 0.78$ PES for the F + CD_4 isotopic variant of the reaction are presented in Figure 5. In one case (solid squares), no restrictions were made with regard to the internal energy content

TABLE 7: Relative Vibrational Populations of the HF Product for the F + CH_4 Reaction at 1.8 kcal mol^{-1} Collision Energy

reference	$v' = 0$	$v' = 1$	$v' = 2$	$v' = 3$	$v' = 4$
Troya et al.[18]	0.00	0.10	0.72	0.18	0.00
Harper et al.[3]	0.04 ± 0.04	0.19 ± 0.03	0.67 ± 0.02	0.11 ± 0.01	
this work MP−SAC2	0.20	0.23	0.29	0.22	0.06
this work MP2	0.21	0.24	0.30	0.20	0.05
this work PES−NOSO	0.08	0.63	0.28	0.01	
Shiu et al.			≈0.20	≈0.80	
this work MP-SAC2 (ZPE)	0.01	0.05	0.20	0.54	0.20
this work PES-NOSO (ZPE)	0.05	0.39	0.52	0.04	

TABLE 8: Energy Disposal into HF + CH_3 Products[a]

	MP2	MP-SAC2	MP-SAC2 (ZPE)	PES-NOSO	PES-NOSO(ZPE)
$\langle f_v(CH_3)\rangle$	0.47	0.46	0.27	0.34	0.27
$\langle f_r(CH_3)\rangle$	0.03	0.03	0.03	0.02	0.02
$\langle f_v(HF)\rangle$	0.36	0.35	0.53	0.34	0.40
$\langle f_r(HF)\rangle$	0.06	0.06	0.07	0.16	0.16
$\langle f_t\rangle$	0.08	0.09	0.10	0.14	0.14

[a] The total available energy is 67.26 kcal mol^{-1} in MP2-SAC PES and 57.9 kcal mol^{-1} in PES-NOSO.

of the CH_3 product in the analysis, whereas in the other case (solid diamonds) only those trajectories whose internal energy is lower than or equal to the CH_3 ZPE, were considered. In the same figure, the experimental excitation function by Zhou and co-workers[7] for the F + CD_4 → DF + $CD_3(v = 0)$ reaction is also presented using two different scaling factors to compare with the theoretical $\sigma_r(E_t)$ with and without CH_3 internal energy restriction. It must be remembered that the measurements only provide the relative excitation function. In both cases, the agreement between theory and experiment is considerably better than that for the F + CH_4 case. The shape and absolute values of the present QCT $\sigma_r(E_t)$ for both isotopic variants of the reaction are very similar. They show similar thresholds and, in both cases, the cross section increases smoothly with increasing collision energy after threshold. Similar behavior has been observed for the three-atom F + H_2 and F + D_2 reactions from both theoretical calculations[39,40] and molecular beam experiments.[41,42] The large difference found in the shape of the experimental $\sigma_R(E_t)$ between the F + CH_4 and F + CD_4 reactions is thus remarkable.[7,9] Moreover, for the F + CD_4 reaction, Liu and co-workers found that the excitation functions for the reactions yielding different vibrational states of CH_3 are very similar in shape.[7] The appearance of a sharp maximum after threshold in the experimental $\sigma_R(E_t)$ for the F + CH_4 reaction is apparently related to the predominance of the channel of the reaction yielding HF($v' = 3$), for which the excitation function shows a prominent maximum at about 2.5 kcal mol^{-1}.[9] This experimental result implies that the most populated v' state of HF in coincidence with vibrationless CH_3 products at collision energies in the range 1−4 kcal mol^{-1} is $v' = 3$. In the present calculations for the title reaction, all the HF(v') state-resolved $\sigma_R(E_t)$ increase smoothly with collision energy (not shown), at variance with the experimental results. The corresponding QCT ICS results using the PES-NOSO surface are also shown in Figure 4. As can be seen, the excitation shows no threshold and its shape is rather different from the experimentally deduced excitation function.

B. HF Vibrational and Rotational Distributions and Energy Disposal. The present HF vibrational populations calculated on the interpolated MP2, MP-SAC2 $F = 0.78$, and PES-NOSO surfaces at 1.8 kcal mol^{-1} collision energy are listed in Table 7 together with the previous QCT data by Troya et al.[18] and the available experimental results. The QCT data corresponding to the reaction yielding CH_3 products with internal energy below or equal its ZPE are also listed in the Table.

As can be seen, the present QCT calculations on the MP2 and MP-SAC2 PESs predict a noticeably population in HF($v' = 0$) that is not observed in any of the experiments or in previous QCT calculations. Although $v' = 2$ is predicted to be slightly more populated (30%) than the rest of the vibrational levels, the differences in population are quite small, even for $v' = 0$. Note that MP2 and MP-SAC2 PESs yield very similar vibrational distributions despite the fact that the MP-SAC2 overestimates considerably the exothermiticy of the reaction. The calculations using the PES-NOSO surface predict that $v' = 1$ is the most populated state followed by $v' = 2$. This is in clear discrepancy with the various experimental data, as well as with the previous QCT results considering the CH_3 as an atom. The overpopulation of the HF($v' = 0$) state obtained in the present full dimensional QCT calculations on the MP2 and MP-SAC2 PESs may be attributed to the high internal energy predicted for the CH_3 coproduct, as can be appreciated in Table 8, where the fractions of the available energy channelled into vibration and rotation of the CH_3 product are listed. In contrast with this result, the experiments of Sugawara et al.[5] and Shiu et al.[10] indicate that only a small portion of the available energy is released as CH_3 internal energy. Furthermore, as observed by Lin et al. for the F + CD_4 reaction,[6] as the CD_3 vibrational energy increases, the DF internal energy decreases. This would confirm that the excess of population into $v' = 0$, and possibly into $v' = 1$, in the present QCT calculations using the MP2 and MP-SAC2 PESs is due to the high internal energy acquired by the CH_3 coproduct, which, in turn, may be produced by deficiencies of the present PESs or shortcomings of the QCT methodology. It may be the case that a leakage of CH_4 zero-point energy in the QCT calculations can be responsible for the high internal energy of the CH_3 coproduct.

However, an inverted vibrational distribution is obtained on the MP-SAC2 PES, with HF($v' = 3$) being the most populated vibrational state, when only trajectories leading to CH_3 with internal energy equal to or below the ZPE are considered. This is in qualitative agreement with the experimental pair-correlated HF vibrational distribution measured for the F + CH_4 → HF(v') + $CH_3(v = 0)$ reaction by Shiu et al.[9] A substantial population of HF($v' = 4$) is obtained in the calculations, at variance with the experimental results, and this is most probably related to the larger exothermicity obtained on the MP-SAC2 $F = 0.78$ PES in comparison with the experimental value. In any case, the experimentally observed trend, in which a vibrational distribution peaking at HF($v' = 2$) when all internal states of the CH_3 coproduct are considered changes to a

TABLE 9: Relative Populations of the DF Product

reference	$v'=0$	$v'=1$	$v'=2$	$v'=3$	$v'=4$	$v'=5$
this work MP-SAC2	0.13	0.16	0.23	0.26	0.17	0.05
this work PES-NOSO	0.09	0.50	0.34	0.06	0.001	
MP-SAC2 (ZPE)	0.01	0.02	0.10	0.24	0.38	0.22
PES-NOSO (ZPE)	0.06	0.40	0.44	0.10	0.002	
Liu et al.			0.02	0.33	0.65	

TABLE 10: Energy Disposal into DF + CD_3 Products[a]

	MP-SAC2	MP-SAC2 (ZPE)	PES-NOSO	PES-NOSO(ZPE)
$\langle f_v(CD_3)\rangle$	0.39	0.21	0.30	0.26
$\langle f_r(CD_3)\rangle$	0.04	0.02	0.02	0.02
$\langle f_v(DF)\rangle$	0.35	0.52	0.29	0.32
$\langle f_r(DF)\rangle$	0.05	0.05	0.20	0.22
$\langle f_t\rangle$	0.17	0.20	0.18	0.19

[a] The total available energy is 63.5 kcal mol^{-1} in MP2-SAC PES and 54.1 kcal mol^{-1} in PES-NOSO.

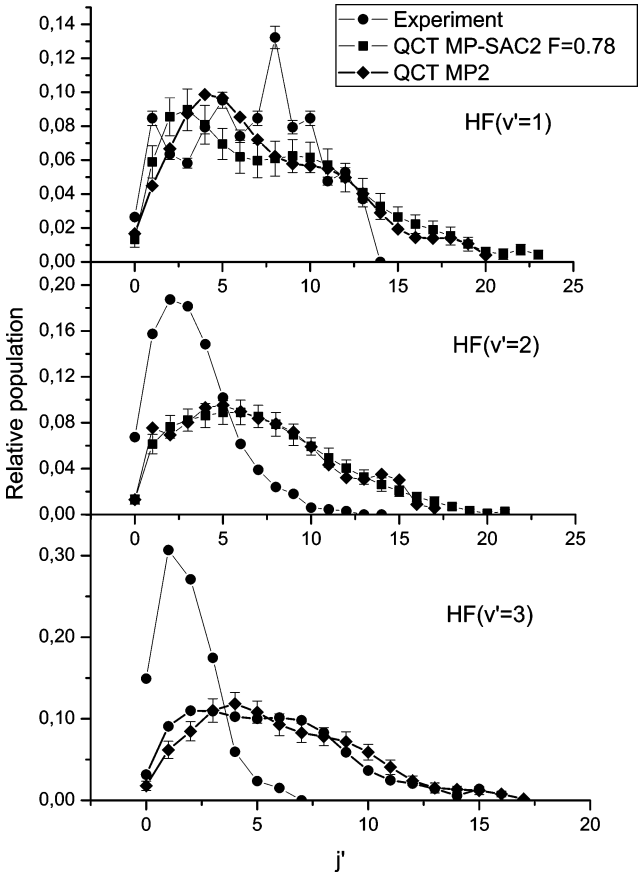

Figure 6. Vibrationally state-resolved HF rotational distributions at $E_t = 1.8$ kcal mol^{-1}. Circles: experimental results from ref 3. Squares: QCT results using the MP-SAC2 $F = 0.78$ PES. Diamonds: QCT results using MP2 PES.

vibrational distribution peaking at HF($v' = 3$) for the reaction producing only $CH_3(v = 0)$ products, is qualitatively reproduced by the present QCT calculations on the MP-SAC2 PES.

Tables 9 and 10 show the present QCT relative vibrational populations for DF and the fractions of the available energy channelled into vibration and rotation of the CD_3 coproduct for the F + CD_4 reaction calculated at 5.4 kcal mol^{-1} collision energy. The results are similar to those corresponding to the F + CH_4 reaction. Once again, a substantial population in DF($v' = 0$) is obtained when the calculations are carried out on the MP-SAC2 $F = 0.78$ PES considering all CH_3 products. However, when only CH_3 molecules with internal energy equal to or below its ZPE are taken into account in the analysis of the trajectories, an inverted vibrational distribution is obtained, with DF($v' = 4$) being the most populated vibrational state, in qualitative agreement with experiment.[6] In this latter case, however, DF molecules in $v' = 5$ are also significantly populated, at variance with experiment (see previous paragraph).

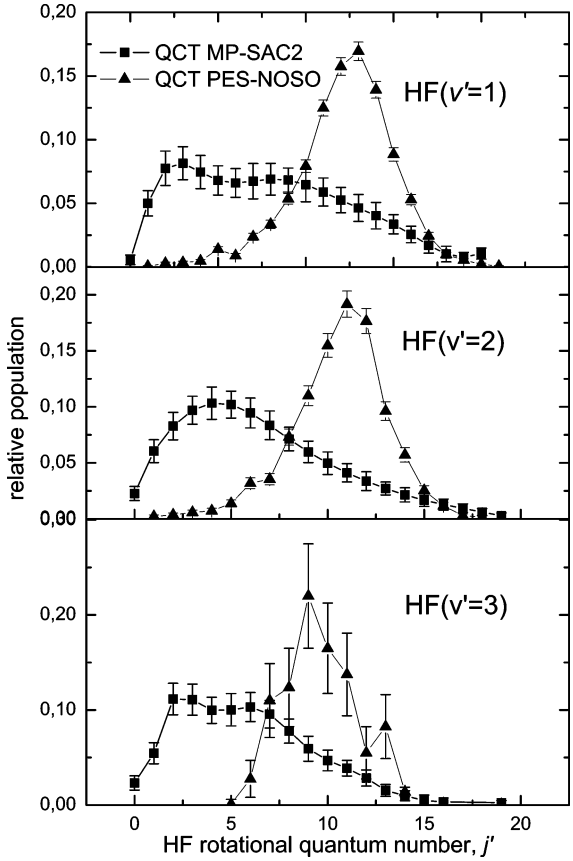

Figure 7. Vibrationally state-resolved HF rotational distributions at $E_t = 1.8$ kcal mol^{-1}. Triangles: QCT results using the PES-NOSO surface.[17] Squares: QCT results using the MP-SAC2 $F = 0.78$ PES.

Figure 6 shows the comparison between the present QCT rotational distributions for HF(v') calculated on the MP2 and MP-SAC2 $F = 0.78$ PESs and those experimentally determined in the experiments of Harper et al.[3] at $E_t = 1.8$ kcal mol^{-1}. As can be seen, there is a reasonable agreement between theory and experiment for HF($v' = 1$). However, the QCT distributions for HF($v' = 2$) and HF($v' = 3$) are significantly hotter than the experimental ones, especially for HF($v' = 3$). For these vibrational states, the theoretical distributions show long tails extending to high j' values, which are absent in the experimental determinations. As the HF vibrational quantum number increases, the rotational distribution becomes colder, in qualitative agreement with the experimental observations. It must be pointed out that the QCT rotational distributions obtained with the MP2 and MP-SAC PESs are very similar despite the larger exothermicity of the latter (see Table 1).

Figure 7 displays the QCT rotational distributions for HF(v') calculated on the MP-SAC2 $F = 0.78$ PES and using the PES-NOSO surface. The latter surface yields very hot rotational distributions in all the v' states and the agreement with the experimental populations is clearly poorer.

The corresponding DF(v') rotational distributions for the F + $CD_4 \rightarrow$ DF + CD_3 reaction at $E_t = 5.4$ kcal mol^{-1} are shown in Figure 8. Although there are not experimental data for this isotopic variant of the reaction, same degree of disagreement between theory and experiment is expected as that obtained for

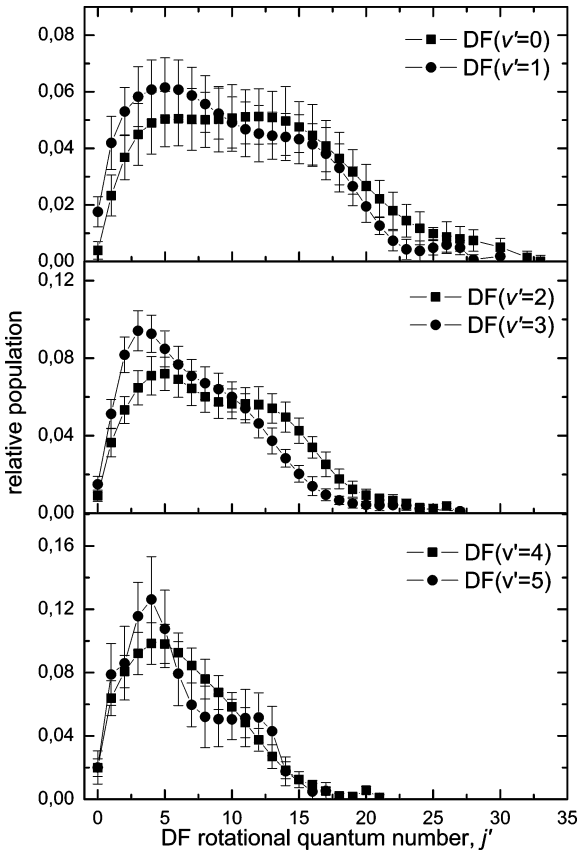

Figure 8. QCT vibrationally state-resolved DF rotational distributions calculated on the MP-SAC2 $F = 0.78$ PES at $E_t = 5.4$ kcal mol^{-1}.

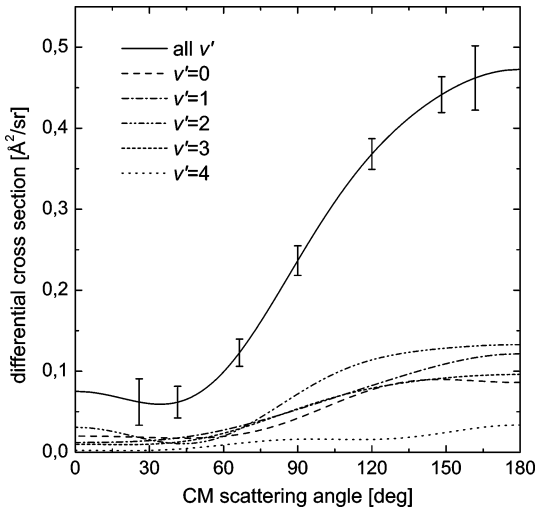

Figure 9. Total and HF vibrationally state-resolved differential cross sections calculated for the F + CH_4 → HF + CH_3 reaction on the MP-SAC2 $F = 0.78$ PES at $E_t = 1.8$ kcal mol^{-1}.

the F + CH_4 reaction. As for the F + CH_4 reaction, in this case the rotational distributions become colder as v' state of DF increases. Some hint of bimodality is observed in the calculated rotational distributions, especially for DF products in $v' = 0-3$.

C. Differential Cross Sections. The QCT total and HF vibrationally state-resolved (regardless of the CH_3 final state) DCSs calculated on the MP-SAC2 $F = 0.78$ PES for the F + CH_4 reaction at 1.8 kcal mol^{-1} collision energy are depicted in Figure 9. As can be seen, the scattering predominantly appears in the backward hemisphere with a small contribution in forward regions. All the state-resolved HF(v') DCSs show similar

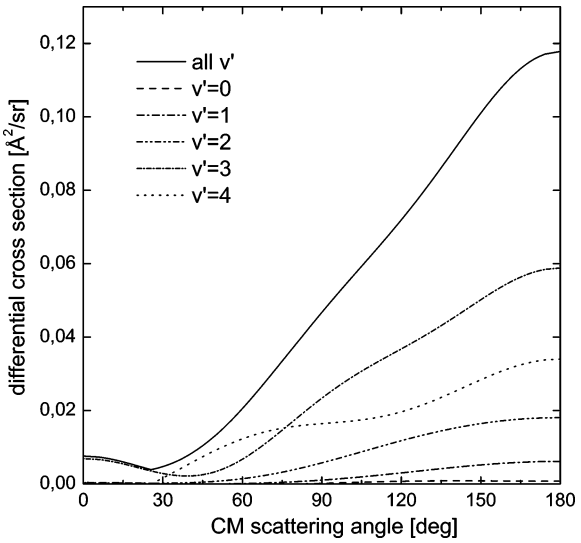

Figure 10. Same as in Figure 9, but considering only those reactive trajectories yielding CH_3 products with internal energy no larger than the ZPE.

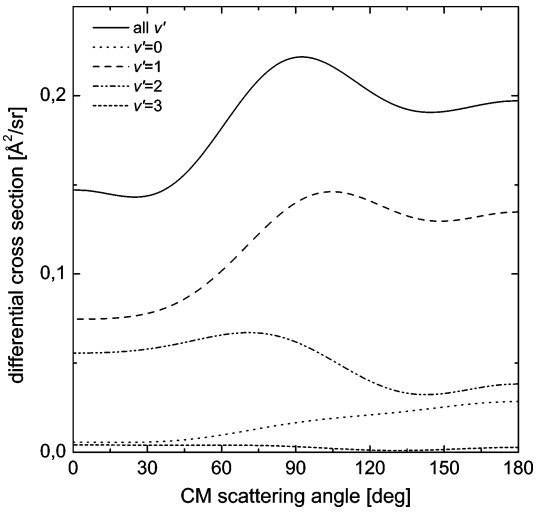

Figure 11. Total and HF vibrationally state-resolved differential cross sections calculated for the F + CH_4 → HF + CH_3 reaction on the PES-NOSO at $E_t = 1.8$ kcal mol^{-1}.

characteristics; i.e., the angular distributions are practically state-independent in the present QCT calculations.

The reduced dimensionality QCT calculations by Troya et al.[18] predicted forward scattering for HF($v' = 3$) and forward−backward symmetry for HF($v' = 2$) and HF($v' = 1$). Experimental studies by Harper and co-workers[4] elucidated a propensity for forward/backward versus sideways scattering in the HF($v' = 1, 2$) manifolds. Liu and co-workers have measured state-resolved, pair-correlated angular distributions for the F + CD_4 → DF(v') + CD_3($v_{1,2,3,4} = 0, 0-3, 0, 0$) reactions at 5.4 kcal mol^{-1},[6,11] showing that the less exoergic products DF($v' = 4$) are forward scattered and the DF($v' = 3$) products spread over all angles and products in DF($v' = 2$) are mainly backward scattered. Thus, for the F + CH_4 → HF(v') + CH_3 reaction at 1.8 kcal mol^{-1}, it is expected that the HF($v' = 3$) should appear in the forward direction and the HF($v' = 2$) products should have a broad distribution in scattering angles. Figure 10 shows the state-resolved HF(v') DCSs calculated considering only the trajectories leading to CH_3 with internal energy no larger than its ZPE. It is interesting to note that in this case only the HF($v' = 3$) products show a small forward component, although the angular distribution is dominated by sideways and backward

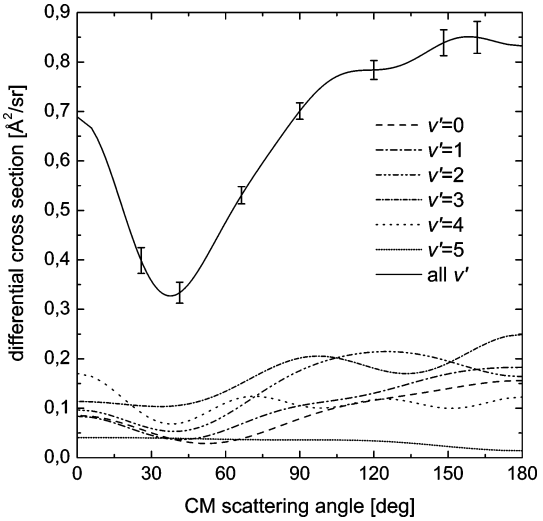

Figure 12. Total and DF vibrationally state-resolved differential cross sections calculated for the $F + CD_4 \rightarrow DF + CD_3$ reaction on the MP-SAC2 $F = 0.78$ PES at $E_t = 5.4$ kcal mol^{-1}.

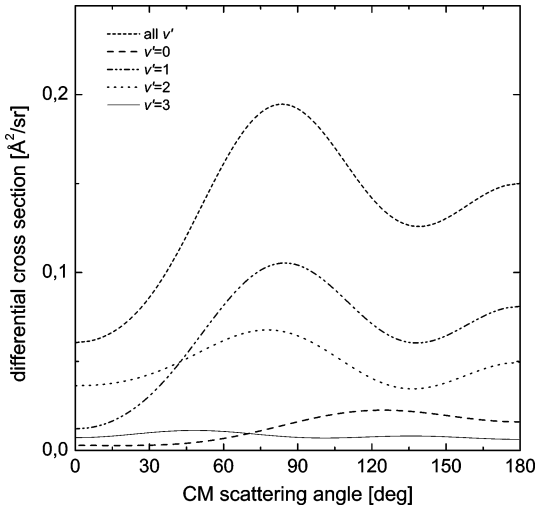

Figure 13. Total and DF vibrationally state-resolved differential cross sections calculated for the $F + CD_4 \rightarrow DF + CD_3$ reaction on the PES-NOSO at $E_t = 5.4$ kcal mol^{-1}.

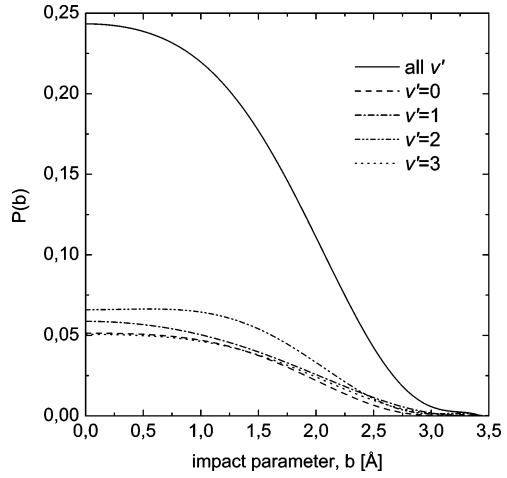

Figure 14. Total and vibrationally state-resolved opacity functions calculated for the $F + CH_4 \rightarrow HF + CH_3$ reaction on the MP-SAC2 $F = 0.78$ PES at $E_t = 1.8$ kcal mol^{-1}.

scattering. For the HF($v' = 1, 2$) products, backward DCSs are obtained, as expected. However, the large contribution from HF($v' = 4$), with a backward−sideways DCS, is at variance with

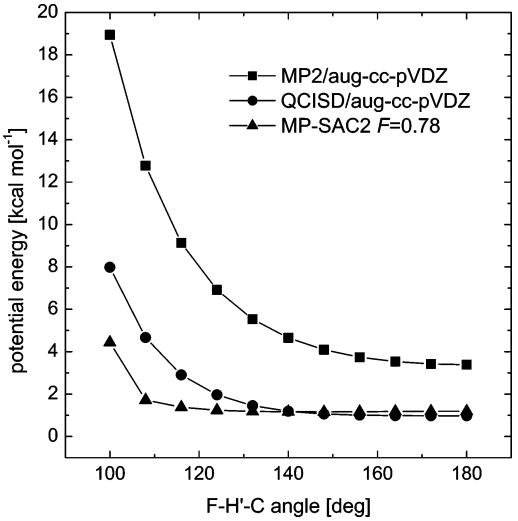

Figure 15. Potential energy as a function of the F−H′-C bending angle in the transition state. Squares: MP2/aug-cc-pVDZ. Circles: QCISD/aug-cc-pVDZ. Triangles: MP-SAC2 $F = 0.78$ (see text for details).

the experimental results, where no evidence of population of this state is found. Figure 11 depicts the DCSs calculated on the PES-NOSO surface that can be compared with those shown in Figure 9. One can see that the shapes of the DCSs are dependent on the HF(v') state and they become increasingly forward shaped as the vibrational state increases. This behavior is in qualitative agreement with the observed angular distributions.[9]

The corresponding QCT DCS calculated on the MP-SAC2 PES for the $F + CD_4 \rightarrow DF + CD_3$ at 5.4 kcal mol^{-1} are shown in Figure 12. The total DCS exhibits a forward peak, but the backward component is much more pronounced than the experimentally observed.[6] Again, the DF state-resolved DCSs show similar shapes for every v' state, whereas, experimentally, every DF v' state is characterized by a different angular distribution, the $v' = 4$ one showing a strong forward peak that dominates the overall DCS. The present QCT calculations on the MP-SAC2 $F = 0.78$ PES cannot reproduce these experimental observations. Figure 13 shows the DF v' DCSs obtained with the PES-NOSO surface. As can be seen, the DCSs look very similar to the corresponding HF(v') DCSs calculated on the same surface.

Inspection of the opacity functions, i.e., the reaction probability as a function of the impact parameter, justifies these findings. Figure 14 shows the total and HF vibrational state-specific opacity functions for the $F + CH_4$ reaction calculated on the MP-SAC2 $F = 0.78$ PES at 1.8 kcal mol^{-1} collision energy. As in the case of the DCSs, there are no differences in the vibrationally state-specific opacity functions and their shapes correspond to that expected for a direct reaction with a F−H′−C collinear transition state. In particular, for $v' = 3$, no hint of a larger participation of high impact parameters is found, hence explaining the small, vibrationally nonspecific forward scattering in the DCS. Figure 15 depicts the potential energy profile as a function of the F−H′−C bending angle, keeping the remaining bond distances and angles frozen to the transition state geometry for the different PESs. As can be seen, the bending potentials calculated at the QCISD/aug-cc-pVDZ ab initio level of theory and for the MP-SAC2 $F = 0.78$ PES are quite flat, whereas that calculated for the MP2/aug-cc-pVDZ PES is steeper. Actually, the shape of the bending potential of the MP-SAC2 $F = 0.78$ PES resembles that of the Stark−Werner ab initio PES for the $F + H_2$ reaction, even though in this latter case the

bending potential showed a clear minimum at the angular configuration of 120°, 0.23 kcal mol^{-1} below the collinear barrier.[43] In the case of the F + H_2 system, it was proved that the shape of the bending potential and the height of the barrier was crucial to obtain forward scattering from QCT and QM calculations.[44,45] Thus, a bending potential for the title reaction more similar to the one for the FH_2 system would yield, in principle, more forward scattering and probably be state-specific. It is also surprising that despite an small early barrier, with a minimum energy path similar to that of the FH_2 system (see Figure 1) there is no clear vibrational population inversion except in the case in which only the trajectories with energy below or equal to the ZPE of the CH_3 are considered.

V. Conclusions

The dynamics of the F + CH_4 → HF + CH_3 and F + CD_4 → DF + CD_3 reactions have been studied by means of quasiclassical trajectory calculations on a new ab initio potential energy surface calculated at the MP2/aug-cc-pVDZ and MP-SAC2 levels of theory using the iterative and interpolation methods implemented in the GROW package by Collins and co-workers. To our knowledge, this is the first study of the title reaction that employs a fully ab initio PES considering all degrees of freedom. QCT calculations have also been performed using the full dimensional semiempirical surface, PES-NOSO, constructed by Espinosa-Garcia and co-workers.[17]

The calculated total reaction cross sections versus collision energy or excitation function for the F + CH_4 reaction does not reproduce well the experimentally observed behavior[9] for the title reaction. However, good correspondence with previous QCT studies[18] is found. For the F + CD_4 reaction the QCT total excitation function calculated with the MP2-SAC PES is in better agreement with experiment.

The present QCT calculations using the MP-SAC2 interpolated PES predict that the accessible HF vibrational levels are roughly equally populated, with some small preponderance of $v' = 2$. The present HF vibrational populations are quantitatively at odds with the experimental determinations and previous QCT calculations, which consider the CH_3 moiety as an atom. We have observed that the HF vibrational populations depend strongly on the amount of vibrational energy disposed in the CH_3 coproduct. Actually, the present QCT calculations give rise to a disposal of vibrational energy nearly equally distributed among the accessible CH_3 and HF vibrational states. Possibly this feature is due to a limitation of the QCT method. The HF($v' = 2, 3$) rotational distributions are *hotter* than the experimental distributions. Finally, the total DCS for the reaction at $E_t = 1.8$ kcal mol^{-1} is mainly backward shaped with a small component in the forward direction. The HF(v') state-resolved DCSs are all similar in shape; i.e., there is no specificity among the different vibrational states of HF. Our QCT calculations using the PES-NOSO semiempirical surface, which reproduces quite well the experimental rate constants and kinetic isotopic effect for the F + CH_4/CD_4,[17] do not yield results in better agreement with the experimental data.

Despite the important discrepancies with the experimental data, the present ab initio and QCT dynamical calculations can be considered as a first step towards the understanding of the dynamics of this complex reaction. To further improve the agreement with the experimental results and to explain in detail the interesting findings derived from the most recent experiments, higher level ab initio calculations for the PES and/or the concurrence of quantum mechanical scattering calculations may be required.

Acknowledgment. J.F.C., E.M.N. and A.F.R. acknowledge support from the Spanish Ministry of Education and Science through the program "Ramón y Cajal". Part of this work has been financed by DGES of Spain (Project BQU2002-04627-C02-02).

References and Notes

(1) Nazar, M. A.; Polanyi, J. C. *Chem. Phys.* **1981**, *55*, 299.
(2) Wickramaaratchi, M. A.; Setser, D. W.; Hildebrandt, H.; Korbitzer, B.; Heydtmann, H. *Chem. Phys.* **1985**, *90*, 109.
(3) Harper, W. W.; Nizkorodov, S. A.; Nesbitt, D. J. *J. Chem. Phys.* **2000**, *113*, 3670.
(4) Harper, W. W.; Nizkorodov, S. A.; Nesbitt, D. J. *Chem. Phys. Lett.* **2001**, *335*, 381.
(5) Sugawara, K.; Ito, F.; Nakagana, T.; Takeo, H.; Matsumura, C. *J. Chem. Phys.* **1990**, *92*, 5328.
(6) Lin, J. J.; Zhou, J.; Shiu, W.; Liu, K. *Science* **2003**, *300*, 966.
(7) Zhou, J.; Lin, J. J.; Shiu, W.; Pu, S.; Liu, K. *J. Chem. Phys.* **2003**, *119*, 2538.
(8) Zhou, J.; Lin, J. J.; Shiu, W.; Liu, K. *J. Chem. Phys.* **2003**, *119*, 4997.
(9) Shiu, W.; Lin, J. J.; Liu, K.; Wu, M.; Parker, D. H. *J. Chem. Phys.* **2004**, *120*, 117.
(10) Shiu, W.; Lin, J. J.; Liu, K. *Phys. Rev. Lett.* **2004**, *92*, 103201.
(11) Zhou, J.; Shiu, W.; Lin, J. J.; Liu, K. *J. Chem. Phys.* **2004**, *120*, 5863.
(12) Zhou, J.; Lin, J. J.; Liu, K. *J. Chem. Phys.* **2004**, *121*, 813.
(13) Corchado, J. C.; Espinosa-Garcia, J. *J. Chem. Phys.* **1996**, *105*, 3152.
(14) Corchado, J. C.; Espinosa-Garcia, J. *J. Chem. Phys.* **1996**, *105*, 3160.
(15) Kornweitz, H.; Persky, A.; Levine, R. D. *Chem. Phys. Lett.* **1998**, *289*, 125.
(16) Okuno, Y.; Yokoyama, S.; Mashiko, S. *J. Chem. Phys.* **2000**, *113*, 3136.
(17) Rangel C, Navarrete M, Espinosa-Garcia, J. *J. Phys. Chem. A* **2005**, *109*, 1441.
(18) Troya, D.; Millan, J.; Baños, I.; Gonzalez, M. *J. Chem. Phys.* **2004**, *120*, 5181.
(19) *JANAF Thermochemical Tables*, 3rd. ed.; Chase, M. W., Davies, C. A., Downey, J. R., Frurip, D. J., McDonald, R. A., Syverud, A. N., Eds.; National Bureau of Standards: Washington, DC, 1985; Vol. 14.
(20) Meredith, J. T.; Jordan M.; Gilbert R. G. *J. Chem. Phys.* **1995**, *102*, 5669.
(21) Jordan, M. J. T.; Thompson, K. C.; Collins, M. A. *J. Chem. Phys.* **1995**, *102*, 5647.
(22) Thompson, K. C.; Jordan, M. J. T.; Collins, M. A. *J. Chem. Phys.* **1998**, *108*, 8302.
(23) Bettens, R. P. A.; Collins, M. A. *J. Chem. Phys.* **1999**, *111*, 816.
(24) Collins, M. A. *Theor. Chem. Acc.* **2002**, *108*, 313.
(25) Frisch, M. J.; Trucks, G. W.; Schlegel, H. B.; Scuseria, G. E.; Robb, M. A.; Cheeseman, J. R.; Zakrzewski, V. G.; Montgomery, J. A., Jr.; Stratmann, R. E.; Burant, J. C.; Dapprich, S.; Millam, J. M.; Daniels, A. D.; Kudin, K. N.; Strain, M. C.; Farkas, O.; Tomasi, J.; Barone, V.; Cossi, M.; Cammi, R.; Mennucci, B.; Pomelli, C.; Adamo, C.; Clifford, S.; Ochterski, J.; Petersson, G. A.; Ayala, P. Y.; Cui, Q.; Morokuma, K.; Malick, D. K.; Rabuck, A. D.; Raghavachari, K.; Foresman, J. B.; Cioslowski, J.; Ortiz, J. V.; Stefanov, B. B.; Liu, G.; Liashenko, A.; Piskorz, P.; Komaromi, I.; Gomperts, R.; Martin, R. L.; Fox, D. J.; Keith, T.; Al-Laham, M. A.; Peng, C. Y.; Nanayakkara, A.; Gonzalez, C.; Challacombe, M.; Gill, P. M. W.; Johnson, B. G.; Chen, W.; Wong, M. W.; Andres, J. L.; Head-Gordon, M.; Replogle, E. S.; Pople, J. A. *Gaussian 98*, revision A.9; Gaussian, Inc.: Pittsburgh, PA, 1998.
(26) Dunning, T. H., Jr. *J. Chem. Phys.* **1989**, *90*, 1007.
(27) Thompson, K. C.; Collins, M. A. *J. Chem. Soc., Faraday Trans.* **1997**, *93*, 871.
(28) Ischtwan, J.; Collins, M. A. *J. Chem. Phys.* **1994**, *100*, 8080.
(29) Jordan, M. J.; Thompson, K. C.; Collins, M. A. *J. Chem. Phys.* **1995**, *102*, 9669.
(30) Hase, W. L.; et al. *QCPE* **1996**, *16*, 671.
(31) Gordon, M. S.; Truhlar, D. G. *J. Am. Chem. Soc.* **1986**, *108*, 5412.
(32) Fast, P. L.; Corchado, J.; Sanchez, M−L.; Truhlar, D. G. *J. Phys. Chem. A* **1999**, *103*, 3139.
(33) Yu, H.-G.; Muckerman, J. T. *J. Phys. Chem. A* **2004**, *108*, 8615.
(34) Castillo, J. F.; Aoiz, F. J.; Bañares, L.; Santamaría, J. *Chem. Phys. Lett.* **2000**, *329*, 517.
(35) Castillo, J. F.; Aoiz, F. J.; Bañares, L. *Chem. Phys. Lett.* **2002**, *356*, 102.
(36) Castillo, J. F.; Collins, M. A.; Aoiz, F. J.; Bañares, L. *J. Chem. Phys.* **2003**, *118*, 7303.

(37) Castillo, J. F.; Aoiz, F. J.; Bañares, L.; Collins, M. A. *J. Phys. Chem. A* **2004**, *108*, 6611.
(38) Notice that the integral cross sections reported in ref 18 have been multiplied by an statistical factor of 4 to account for the fact that only one of the four equivalent hydrogen atoms of CH_4 is reactive in their reduced-dimensionality approach.
(39) Aoiz, F. J.; Bañares, L.; Herrero, V. J.; Stark, K.; Werner, H.-J. *Chem. Phys. Lett.* **1996**, *254*, 341.
(40) Aquilanti, V.; Cavalli, S.; De Fazio, D.; Volpi, A.; Aguilar, A.; Gimémez, X.; Lucas, J. M. *Chem. Phys. Lett.* **2003**, *371*, 504.
(41) Dong, F.; Lee, S.-H.; Liu, K. *J. Chem. Phys.* **2000**, *113*, 3633.
(42) Aoiz, F. J.; Bañares, L.; Castillo, J. F. Unpublished results.
(43) Stark, K.; Werner, H.-J. *J. Chem. Phys.* **1996**, *104*, 6515.
(44) Aoiz, F. J.; Bañares, L.; Herrero, V. J.; Sáez Rábanos, V.; Stark, K.; Werner, H.-J. *Chem. Phys. Lett.* **1994**, *223*, 215.
(45) Castillo, J. F.; Hartke, B.; Werner, H.-J.; Aoiz, F. J.; Bañares, L.; Martínez-Haya, B. *J. Chem. Phys.* **1998**, *109*, 7224.
(46) Persky, A. *J. Phys. Chem.* **1996**, *100*, 689.
(47) Berkowitz, J.; Ellison, G. B.; Gutman, D. *J. Phys. Chem.* **1994**, *98*, 2744.